AIAA Aviation
16-20 June 2014, Atlanta, GA
20th AIAA/CEAS Aeroacoustics Conference

Theoretical Study and Numerical Validation of Sound Radiation from Coaxial Annular Duct

Xin Liu* and Xun Huang†
Peking University, Beijing, 100871, People's Republic of China

Theoretical solutions and numerical verification are developed and conducted in this work for spinning mode sound radiation from semi-infinite annular duct. Our problem is different from previous works in that both its inner pipe and outer pipe are semi-infinite. Hence, this problem is a better representative of aircraft engine bypass duct. The associated theoretical developments with mathematical tools, such as Wiener-Hopf matrix and its factorization, become complicated and need extra examination. Instability resulting from two coupled vortex sheets is investigated. Khrapkov commutative factorization is utilized to fulfill the matrix splitting. A direct computation of the wave model governed by linearized Euler equations is performed here using high order schemes to verify the proposed theoretical solutions. The results of the theoretical solutions and numerical computations are compared in the paper. The results show that in both near- and far-field, the theoretical model we have built is indeed a fairly good model for the very problem, which could be numerically simulated in a faster and more robust way.

I. Introduction

Fan is one of the most critical sound sources from modern high bypass turbofan engines, which include a bypass duct and a core duct. The acoustic source travels along the bypass duct and then radiates into the exterior space, with the influence of the velocity mismatches between different layers of flow. The flow speed of the bypass duct is higher than the ambient flow speed. And the jet flow speed of the central core duct is much higher than the rest flow speeds. Lots of efforts have been paid to provide an analytical solution for an idealized description of such problems, which could be taken as an useful engineering model.

By using Weiner-Hopf technique on sound radiation problem from a semi-infinite cylindrical duct, Levine and Schwinger[1] have provided a systematical way for such half-range diffraction problems. However, special treatment needs to be paid for flow that is directed out of the duct since at the trailing edge singularity occurs with vortex sheet. Carrier[2] and Munt[3] presents the importance of vortex sheet for acoustic field. Reinstra[4] demonstrates the complexity of the interaction between sound radiation and vortex shedding. Solutions with limitations have been discussed, for instance small Strouhal number[4] and low or high frequencies.[5,6]

Kelvin-Helmholtz instability has theoretical significance for diffraction problems involving an unstable shear layer shedding from surface edge. Morgan[7] and Crighton & Leppington[8] studied sound radiation from a semi-infinite flat plate independently and showed that an instability in vortex sheet is excited by incident disturbance which leads to a large amplitude wave (the instability wave) in acoustic field.

Moreover, in order to satisfy causality problem, rigorous approaches have to be taken into consideration. Morgan[7] found that only solutions satisfying "full Kutta condition" makes the edge velocity finite, which is demonstrated experimentally by Bechert and Pfizenmaier[9] under thin shear layer condition.

Munt[3] have studied the radiation of sound through a vortex sheet emanating from a circular pipe. Reinstra[4] derived the general solution for a semi-infinite duct with an infinite center body in the case of a uniform flow and Gabard and Astley[10] extends this work to a more generic case with a non-uniform flow. All these previous works utilize a mathematical tool, the Weiner-Hopf method,[11] systematically for various duct radiation problems. The essential technologies of these previous investigations inspire our study.

*PhD student, Department of Mechanics & Aerospace Engineering, College of Engineering, Peking University. Email: liuxinonly@pku.edu.cn.

†Professor. Affiliations: (1) Department of Aeronautics and Astronautics; and (2) State Key Laboratory of Turbulence and Complex Systems. AIAA Senior Member. Email: huangxun@pku.edu.cn.

A theoretical solution is presented in this work that describes the time harmonic spinning mode sound radiation from an axisymmetric annular duct, where both the outer and inner pipes are semi-infinite (see figure. 1(c)). The inner core duct contains the jet flow and the outer bypass duct contains the bypass airflow. In the cases we mentioned above, the geometries are quite simple that Weiner-Hopf equations are scalar. While in our case, we elucidate inherent mathematic modeling using Wiener-Hopf matrix, which makes the kernel decomposition difficult. Taylor, Crighton and Cargill[12] derived an approximation solution for nozzle case by solving the two semi-infinite geometries separately. Therefore only scalar Weiner-Hopf techniques are used. Veitch and Peake[13] derive an solution by applying matrix Weiner-Hopf techniques for sound scattering in the exhaust flow from coaxial cylinders, where the inner pipe could be either buried inside the outer cylinder or protrude downstream beyond the outer pipe end. Our case has the similar geometry with Veich and Peake but different matrix Weiner-Hopf techniques are used. All the corresponding geometrical setups are shown in figure.1(a-b), respectively.

The proposed theoretical solutions are validated using high confidence linearized Euler equations (LEE) model and computational aeroacoustic (CAA) tools.[14] Our research provides a new classical benchmark for CAA and deep insights of the relevant physics. Once the model is confirmed to be accurately, it could be used as a tool of verification for other theoretical or numerical work.[15–17]

II. Statement of the problem

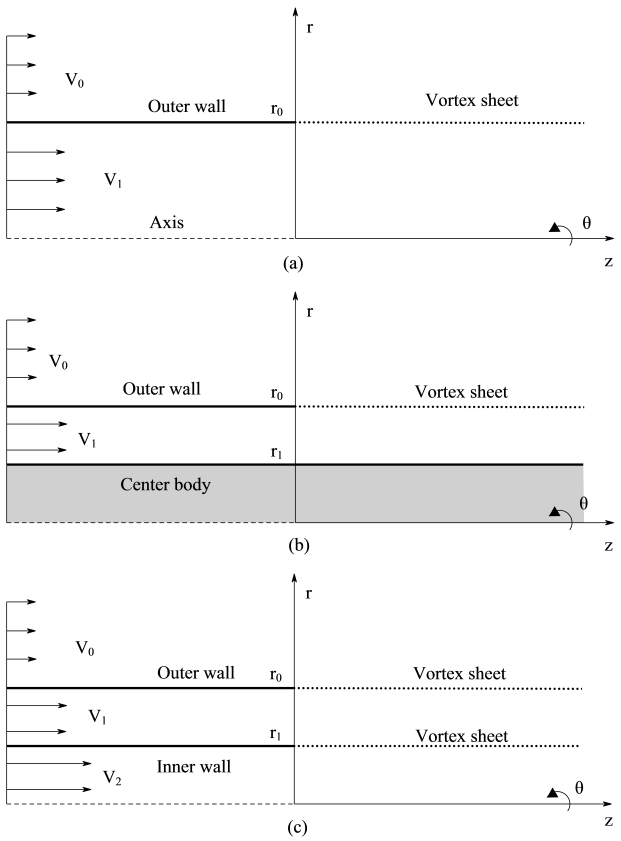

Figure 1. Geometrical setups of: (a)Munt's case,[3] (b)Gabard and Astley's case,[10] (c) Our case.

In this work all equations are described within cylindrical coordinates (r, θ, z). As in figure 1(c), the outside pipe of radius r_0 and the inside pipe of the radius r_1 are infinite as $z \to -\infty$. Both surfaces of the pipes are rigid and impervious, with an idealized outer wall of idealized zero thickness. The inner pipe contains a uniform mean flow with density ρ_2, velocity v_2, speed of sound c_2, while another uniform mean flow with density ρ_1, velocity v_1, speed of sound c_1 exists in the space between inner and outer pipe. Outside the pipes there is an ambient flow with density ρ_0, velocity v_0 and speed of sound c_0.

Next we construct the governing equations. Assuming the flow is irrotational except the vortex sheet, a velocity potential is introduced that satisfies the nondimensional Helmholtz equation with reference values ρ_0, p_0, c_0, r_0.

$$(\frac{\partial}{\partial t}+M_0\frac{\partial}{\partial z})^2\phi-\Delta\phi=0, \qquad r>1, \tag{1}$$

$$C_1^2(\frac{\partial}{\partial t}+M_1\frac{\partial}{\partial z})^2\phi-\Delta\phi=0, \qquad h<r<1, \tag{2}$$

$$C_2^2(\frac{\partial}{\partial t}+M_2\frac{\partial}{\partial z})^2\phi-\Delta\phi=0, \qquad r<h. \tag{3}$$

where $M_0=v_0/c_0$, $M_1=v_1/c_0$, $M_2=v_2/c_0$, $C_1=c_0/c_1$, $C_2=c_0/c_2$, $h=r_1/r_0$.

The acoustic pressure p, velocity $\vec{v}$ and density ρ are given by:

$$p=-(\frac{\partial\phi}{\partial t}+M_0\frac{\partial\phi}{\partial z}), \qquad \vec{v}=\nabla\phi, \qquad \rho=p, \qquad r>1, \tag{4}$$

$$p=-D_1(\frac{\partial\phi}{\partial t}+M_1\frac{\partial\phi}{\partial z}), \qquad \vec{v}=\nabla\phi, \qquad \rho=pC_1^2, \qquad h<r<1 \tag{5}$$

$$p=-D_2(\frac{\partial\phi}{\partial t}+M_2\frac{\partial\phi}{\partial z}), \qquad \vec{v}=\nabla\phi, \qquad \rho=pC_2^2, \qquad r<h. \tag{6}$$

where $D_1=\rho_1/\rho_0$, $D_2=\rho_2/\rho_0$.

Our problem include four kinds of boundary conditions:

(1) Rigid Walls

At the rigid walls, the boundary conditions are given by:

$$\frac{\partial\phi}{\partial r}(1^{\pm},\theta,z)=\frac{\partial\phi}{\partial r}(h^{\pm},\theta,z)=0, \quad z\le 0. \tag{7}$$

(2) Symmetry

$$\frac{\partial\phi}{\partial r}(0,\theta,z)=0. \tag{8}$$

(3) Displacement continuity

Assuming $w_1(\theta,z)$ and $w_2(\theta,z)$ are the displacements of the vortex sheets at R_1 and R_2, the acceleration of which represents the velocity at the very location. Then $w_1(\theta,z)$ and $w_2(\theta,z)$ yield

$$(\frac{\partial}{\partial t}+M_0\frac{\partial}{\partial z})w_1(\theta,z)=\frac{\partial\phi}{\partial r}(1^+,\theta,z), \quad z\ge 0, \tag{9}$$

$$(\frac{\partial}{\partial t}+M_1\frac{\partial}{\partial z})w_1(\theta,z)=\frac{\partial\phi}{\partial r}(1^-,\theta,z), \quad z\ge 0, \tag{10}$$

$$(\frac{\partial}{\partial t}+M_1\frac{\partial}{\partial z})w_2(\theta,z)=\frac{\partial\phi}{\partial r}(h^+,\theta,z), \quad z\ge 0, \tag{11}$$

$$(\frac{\partial}{\partial t}+M_2\frac{\partial}{\partial z})w_2(\theta,z)=\frac{\partial\phi}{\partial r}(h^-,\theta,z), \quad z\ge 0. \tag{12}$$

(4) Pressure continuity

The pressure at each side of the vortex sheet should be equal:

$$p(1^+,\theta,z)=p(1^-,\theta,z), \quad p(h^+,\theta,z)=p(h^-,\theta,z), \quad z\ge 0, \tag{13}$$

which derive:

$$(\frac{\partial}{\partial t}+M_0\frac{\partial}{\partial z})\phi(1^+,\theta,z,t)=D_1(\frac{\partial}{\partial t}+M_1\frac{\partial}{\partial z})\phi(1^-,\theta,z,t), \quad z\ge 0, \tag{14}$$

$$D_1(\frac{\partial}{\partial t}+M_1\frac{\partial}{\partial z})\phi(h^+,\theta,z,t)=D_2(\frac{\partial}{\partial t}+M_2\frac{\partial}{\partial z})\phi(h^-,\theta,z,t), \quad z\ge 0. \tag{15}$$

We are primarily interested in the acoustic field produced by a wave propagating in the annular pipe towards the exit plane and then radiating in the free field. The form of the solution is time-harmonic and

axial symmetrical, taking the form of $\exp(im\theta - i\omega t)$. Since the geometry and boundary conditions are axisymmetrical, the diffracted field retains the same azimuthal and time dependence as the incident wave. Then the governing equations of $\psi(r,z)$ could be derived, which makes it a two-dimensional problem. We can split the flow field into two parts: incident wave ϕ_i and diffraction field ϕ_d, as the following:

$$\phi(r,\theta,z,t) = \phi_i(r,\theta,z,t) + \phi_d(r,\theta,z,t). \tag{16}$$

With the assumption above, the velocity potential of the diffracted field could be written as

$$\phi_d(r,\theta,z,t) = \psi(r,z)\exp(im\theta - i\omega t), \tag{17}$$

$$\phi_i(r,\theta,z,t) = \psi_i(r,z)\exp(im\theta - i\omega t). \tag{18}$$

It is obvious that for incident wave ψ_i is zero other than in $h < r < 1$ region. When $h < r < 1$, according to the method of separation of variables, we could have:

$$\phi_i(r,\theta,z,t) = \sum_{m=-\infty}^{\infty}\sum_{n=0}^{\infty}[B^+_{mn}\exp(i\omega\mu^+_{mn}z) + B^-_{mn}\exp(i\omega\mu^-_{mn}z)]\cdot\psi_{mn}(r)\exp(im\theta - i\omega t), \tag{19}$$

where

$$\psi_{mn}(r) = \mathrm{Y}'_m(\alpha_{mn}h)\mathrm{J}_m(\alpha_{mn}r) - \mathrm{J}'_m(\alpha_{mn}h)\mathrm{Y}_m(\alpha_{mn}r), \tag{20}$$

$$\mu^{\pm}_{mn} = \frac{\pm\sqrt{C_1 - (1-M_1^2C_1^2)(\alpha_{mn})^2/\omega^2} - M_1C_1^2}{1-M_1^2C_1^2}, \tag{21}$$

and α_{mn} is the n-th solution of characteristic equation

$$\mathrm{J}'_m(\alpha)\mathrm{Y}'_m(\alpha h) - \mathrm{J}'_m(\alpha h)\mathrm{Y}'_m(\alpha) = 0. \tag{22}$$

The wave propagates out of the duct is our main interest therefore we only take the right-going mode μ^+_{mn} into account. Since the incident wave is a superposition of multi-modes, we could consider just one certain mode (m,n).

Similarly, the displacements of the vortex sheets could be written as

$$w_1 = \xi_1(r,z)\exp(im\theta - i\omega t), \quad r = 1, \tag{23}$$

$$w_2 = \xi_2(r,z)\exp(im\theta - i\omega t), \quad r = h. \tag{24}$$

From all above we could obtain the governing equations of $\psi(r,z)$:

$$\left(\frac{1}{r}\frac{\partial}{\partial r}\left(r\frac{\partial}{\partial r}\right) + \frac{\partial^2}{\partial z^2} - \frac{m^2}{r^2}\right)\psi - \left(-i\omega + M_0\frac{\partial}{\partial z}\right)^2\psi = 0, \quad r > 1, \tag{25}$$

$$\left(\frac{1}{r}\frac{\partial}{\partial r}\left(r\frac{\partial}{\partial r}\right) + \frac{\partial^2}{\partial z^2} - \frac{m^2}{r^2}\right)\psi - C_1^2\left(-i\omega + M_1\frac{\partial}{\partial z}\right)^2\psi = 0, \quad h < r < 1, \tag{26}$$

$$\left(\frac{1}{r}\frac{\partial}{\partial r}\left(r\frac{\partial}{\partial r}\right) + \frac{\partial^2}{\partial z^2} - \frac{m^2}{r^2}\right)\psi - C_2^2\left(-i\omega + M_2\frac{\partial}{\partial z}\right)^2\psi = 0, \quad r < h, \tag{27}$$

$$\frac{\partial\psi}{\partial r}(1^{\pm},\theta,z) = \frac{\partial\psi}{\partial r}(h^{\pm},\theta,z) = 0, \quad z \le 0, \tag{28}$$

$$\frac{\partial\psi}{\partial r}(0,\theta,z) = 0, \quad \forall z, \tag{29}$$

$$\left(-i\omega + M_0\frac{\partial}{\partial z}\right)\xi_1(z) = \frac{\partial\psi}{\partial r}(1^+,z), \quad z \ge 0, \tag{30}$$

$$\left(-i\omega + M_1\frac{\partial}{\partial z}\right)\xi_1(z) = \frac{\partial\psi}{\partial r}(1^-,z), \quad z \ge 0, \tag{31}$$

$$\left(-i\omega + M_1\frac{\partial}{\partial z}\right)\xi_2(z) = \frac{\partial\psi}{\partial r}(h^+,z), \quad z \ge 0, \tag{32}$$

$$\left(-i\omega + M_2\frac{\partial}{\partial z}\right)\xi_2(z) = \frac{\partial\psi}{\partial r}(h^-,z), \quad z \ge 0, \tag{33}$$

$$\left(-i\omega + M_0\frac{\partial}{\partial z}\right)\psi(1^+,z) = D_1\left(-i\omega + M_1\frac{\partial}{\partial z}\right)\left[\psi(1^-,z) + \psi_i(1^-,z)\right], \quad z \geq 0, \tag{34}$$

$$D_1\left(-i\omega + M_1\frac{\partial}{\partial z}\right)\left[\psi(h^+,z) + \psi_i(h^+,z)\right] = D_2\left(-i\omega + M_2\frac{\partial}{\partial z}\right)\psi(h^-,z), \quad z \geq 0. \tag{35}$$

Here we have to mention that vorticity could not been determined from the equations above since the viscosity is neglected and the shear layers are of zero thickness. Full Kutta condition are then applied to ensure the pressure at the trailing edge is finite, which yields $\phi(r,z)|_{r=1,h} = O(z^{3/2})$ as $z \to 0$. The detailed discussion could be referred in Reinstra[4] and Garbard.[?]

Jones and Morgan[7, 18–21] have presents a series of work to address the causality problem. In this paper we would briefly reveal the conclusion that during mathematical analysis, solutions under complex frequency with positive imaginary part would satisfy the causality condition.

III. Weiner-Hopf Method

A. Derivation of the kernel equation

A typical Weiner-Hopf problem requires solution of steady state wave equation in free space when semi-infinite boundaries are considered. For our problem, the rigid wall condition is applied for $z < 0$ and continuity condition for $z > 0$.

The half-range Fourier transforms of $\psi(r,z)$ in the axial direction are defined:

$$\beta_+(r,u) = \int_0^{+\infty}\psi(r,z)e^{-i\omega uz}dz, \qquad \beta_-(r,u) = \int_{-\infty}^{0}\psi(r,z)e^{-i\omega uz}dz. \tag{36}$$

The conventional Fourier transform is $\beta = \beta_- + \beta_+$. Applying the transform on Eqs. (25)-(27) we could have:

$$\frac{1}{r}\frac{\partial}{\partial r}\left(r\frac{\partial\beta}{\partial r}\right) + \left(\omega^2\lambda_i^2 - \frac{m^2}{r^2}\right)\beta = 0, \qquad i = 0,1,2, \tag{37}$$

where the axial wavenumbers satisfy the dispersion relations:

$$\lambda_0^2 = (1-uM_0)^2 - u^2, \qquad \lambda_1^2 = C_1^2(1-uM_1)^2 - u^2, \qquad \lambda_2^2 = C_2^2(1-uM_2)^2 - u^2 \tag{38}$$

Then we could write these wavenumbers in the form $\lambda_0 = \lambda_0^+\lambda_0^-$, $\lambda_1 = \lambda_1^+\lambda_1^-$, $\lambda_2 = \lambda_2^+\lambda_2^-$ with

$$\lambda_0^\pm = \sqrt{1-u(M_0 \pm 1)}, \qquad \lambda_1^\pm = \sqrt{C_1 - u(M_1C_1 \pm 1)}, \qquad \lambda_2^\pm = \sqrt{C_2 - u(M_2C_2 \pm 1)}. \tag{39}$$

Here we would like to remind the readers the regularity of $\lambda_i^\pm (i = 0,1,2)$, in the complex plane. Branch cuts are taken from $u_i^\pm$ to $\pm\infty$ for $\lambda_i^\pm$, where $u_0^\pm = 1/(M_0 \pm 1)$, $u_1^\pm = C_1/(M_1C_1 \pm 1)$ and $u_2^\pm = C_2/(M_2C_2 \pm 1)$.

Considering the geometrical condition Eq. (28)(29), and wave vanishing at infinity, $\beta(r,u)$ has the form

$$\beta(r,u) = \begin{cases} A(u)\mathrm{H}_m^{(1)}(\lambda_0\omega r), & r > 1, \\ B(u)\mathrm{J}_m(\lambda_1\omega r) + C(u)\mathrm{Y}_m(\lambda_1\omega r), & h < r < 1, \\ D(u)\mathrm{J}_m(\lambda_2\omega r), & r < h. \end{cases} \tag{40}$$

The discussion of the regularity of the transform β is a necessary step in Weiner-Hopf problem. When $z \to \pm\infty$ the diffracted field behaves like axial plane waves, which according to Noble,[11] $\beta_\pm$ are regular in the half-plane $R_0^\pm$ for $r > 1$, $\beta_\pm$ are regular in the half-plane $R_1^\pm$ for $h < r < 1$, $\beta_\pm$ are regular in the half-plane $R_2^\pm$ for $r < h$ respectively. The half planes are defined as:

$$R_0^\pm: \quad \pm\mathrm{Im}(u-u_0^\pm) < \mp\tan(\epsilon)\mathrm{Re}(u-u_0^\pm), \tag{41}$$

$$R_1^\pm: \quad \pm\mathrm{Im}(u-u_1^\pm) < \mp\tan(\epsilon)\mathrm{Re}(u-u_1^\pm), \tag{42}$$

$$R_2^\pm: \quad \pm\mathrm{Im}(u-u_2^\pm) < \mp\tan(\epsilon)\mathrm{Re}(u-u_2^\pm), \tag{43}$$

where $\epsilon = \mathrm{Im}(\omega)/\mathrm{Re}(\omega), 0 \leq \epsilon \leq \pi/2$. Therefore, we could define a strip $S(R^- < u < R^+)$ that is the intersection of all the half plane, where β is regular for all possible r. In this way, the imaginary parts of $\lambda_i\omega (i = 0,1,2)$, are positive in S. As $r \to +\infty$, β decreases.

Furthermore, to solve the problem of interests we introduce some other transforms:

$$G_1(u) = \int_{-\infty}^{+\infty} \left[\left(-i\omega + M_0 \frac{\partial}{\partial z} \right) \psi(1^+, z) - D_1 \left(-i\omega + M_1 \frac{\partial}{\partial z} \right) \psi(1^-, z) \right] \cdot \exp(-i\omega u z) dz, \tag{44}$$

$$G_2(u) = \int_{-\infty}^{+\infty} \left[D_1 \left(-i\omega + M_1 \frac{\partial}{\partial z} \right) \psi(h^+, z) - D_2 \left(-i\omega + M_2 \frac{\partial}{\partial z} \right) \psi(h^-, z) \right] \cdot \exp(-i\omega u z) dz, \tag{45}$$

$$F_1^+(u) = \int_0^{+\infty} \xi_1(z) \exp(-i\omega u z) dz, \tag{46}$$

$$F_2^+(u) = \int_0^{+\infty} \xi_2(z) \exp(-i\omega u z) dz. \tag{47}$$

By taking advantage of Eq. (34)(35), $G_1^+(u)$ and $G_2^+(u)$ could be integrated directly:

$$\begin{aligned} G_1^+ &= \int_0^{+\infty} D_1 \left(-i\omega + M_1 \frac{\partial}{\partial z} \right) \psi_i(1^-, z) \exp(-i\omega u z) dz \\ &= \frac{D_1(1 - \mu_{mn}^+ M_1)\psi_{mn}(1)}{\mu_{mn}^+ - u} \end{aligned} \tag{48}$$

$$\begin{aligned} G_2^+ &= \int_0^{+\infty} -D_1 \left(-i\omega + M_1 \frac{\partial}{\partial z} \right) \psi_i(h^+, z) \exp(-i\omega u z) dz \\ &= -\frac{D_1(1 - \mu_{mn}^+ M_1)\psi_{mn}(h)}{\mu_{mn}^+ - u} \end{aligned} \tag{49}$$

Applying the transform on Eqs. (30)-(33), the unknown coefficients in Eq. (40) could be represented in the form F_1^+ and F_2^+.

$$A(u) = \frac{-i(1 - uM_0)}{\lambda_0} \cdot \frac{F_1(u)}{\mathrm{H}_m^{(1)\prime}(\lambda_0 \omega)}, \tag{50}$$

$$B(u) = \frac{-i(1 - uM_1)}{\lambda_1} \cdot \frac{\mathrm{Y}_m'(\lambda_1 \omega h) F_1(u) - \mathrm{Y}_m'(\lambda_1 \omega) F_2(u)}{\mathrm{J}_m'(\lambda_1 \omega)\mathrm{Y}_m'(\lambda_1 \omega h) - \mathrm{J}_m'(\lambda_1 \omega h)\mathrm{Y}_m'(\lambda_1 \omega)}, \tag{51}$$

$$C(u) = \frac{i(1 - uM_1)}{\lambda_1} \cdot \frac{\mathrm{J}_m'(\lambda_1 \omega h) F_1(u) - \mathrm{J}_m'(\lambda_1 \omega) F_2(u)}{\mathrm{J}_m'(\lambda_1 \omega)\mathrm{Y}_m'(\lambda_1 \omega h) - \mathrm{J}_m'(\lambda_1 \omega h)\mathrm{Y}_m'(\lambda_1 \omega)}, \tag{52}$$

$$D(u) = \frac{-i(1 - uM_2)}{\lambda_2} \cdot \frac{F_2(u)}{\mathrm{J}_m'(\lambda_2 \omega h)}. \tag{53}$$

Substituting solution Eq. (40) into Eqs. (44)(45), we would have the matrix form of the control equations:

$$\mathbf{G}^+ + \mathbf{G}^- = \frac{\omega}{\lambda_0 \lambda_1 \lambda_2} \mathbf{K} \mathbf{F}^+, \tag{54}$$

where

$$\mathbf{G}^\pm = \begin{pmatrix} G_1^\pm \\ G_2^\pm \end{pmatrix}, \mathbf{F}^+ = \begin{pmatrix} F_1^+ \\ F_2^+ \end{pmatrix}, \mathbf{K} = \begin{pmatrix} K_{11}(u) & K_{12}(u) \\ K_{21}(u) & K_{22}(u) \end{pmatrix}, \tag{55}$$

$$\begin{aligned} K_{11}(u) &= D_1(1 - uM_1)^2 \cdot \lambda_0 \lambda_2 \cdot \frac{\mathrm{J}_m(\lambda_1 \omega)\mathrm{Y}_m'(\lambda_1 \omega h) - \mathrm{J}_m'(\lambda_1 \omega h)\mathrm{Y}_m(\lambda_1 \omega)}{\mathrm{J}_m'(\lambda_1 \omega)\mathrm{Y}_m'(\lambda_1 \omega h) - \mathrm{J}_m'(\lambda_1 \omega h)\mathrm{Y}_m'(\lambda_1 \omega)} \\ &\quad -(1 - uM_0)^2 \cdot \lambda_1 \lambda_2 \cdot \frac{\mathrm{H}_m^{(1)}(\lambda_0 \omega)}{\mathrm{H}_m^{(1)\prime}(\lambda_0 \omega)}, \end{aligned} \tag{56}$$

$$K_{12}(u) = -D_1(1 - uM_1)^2 \cdot \lambda_0 \lambda_2 \cdot \frac{\mathrm{J}_m(\lambda_1 \omega)\mathrm{Y}_m'(\lambda_1 \omega) - \mathrm{J}_m'(\lambda_1 \omega)\mathrm{Y}_m(\lambda_1 \omega)}{\mathrm{J}_m'(\lambda_1 \omega)\mathrm{Y}_m'(\lambda_1 \omega h) - \mathrm{J}_m'(\lambda_1 \omega h)\mathrm{Y}_m'(\lambda_1 \omega)}, \tag{57}$$

$$K_{21}(u) = -D_1(1 - uM_1)^2 \cdot \lambda_0 \lambda_2 \cdot \frac{\mathrm{J}_m(\lambda_1 \omega h)\mathrm{Y}_m'(\lambda_1 \omega h) - \mathrm{J}_m'(\lambda_1 \omega h)\mathrm{Y}_m(\lambda_1 \omega h)}{\mathrm{J}_m'(\lambda_1 \omega)\mathrm{Y}_m'(\lambda_1 \omega h) - \mathrm{J}_m'(\lambda_1 \omega h)\mathrm{Y}_m'(\lambda_1 \omega)}, \tag{58}$$

$$K_{22}(u) = D_1(1-uM_1)^2 \cdot \lambda_0\lambda_2 \cdot \frac{\mathrm{J}_m(\lambda_1\omega h)\mathrm{Y}'_m(\lambda_1\omega) - \mathrm{J}'_m(\lambda_1\omega)\mathrm{Y}_m(\lambda_1\omega h)}{\mathrm{J}'_m(\lambda_1\omega)\mathrm{Y}'_m(\lambda_1\omega h) - \mathrm{J}'_m(\lambda_1\omega h)\mathrm{Y}'_m(\lambda_1\omega)}$$
$$+D_2(1-uM_2)^2 \cdot \lambda_0\lambda_1 \cdot \frac{\mathrm{J}_m(\lambda_2\omega h)}{\mathrm{J}'_m(\lambda_2\omega h)}. \quad (59)$$

The $\mathbf{K}(u)$ is the Weiner-Hopf kernel of the very problem. Comparing with previous cases, two instead of one shear layers occur in the problem, resulting in the kernel being a matrix that represents the coupling of the two scattering field.

B. Properties of the kernel

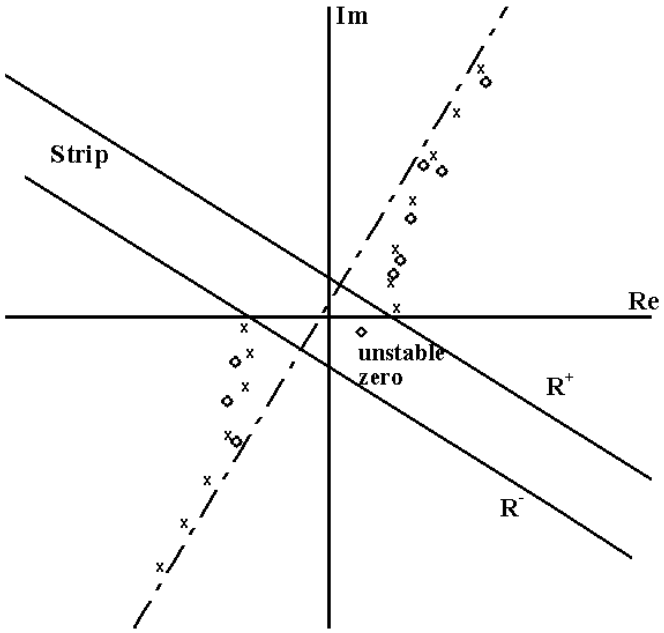

Figure 2. Location of the zeros ∘ and poles × of the kernel. $\omega = 10$, $M_0 = 0.0$, $M_1 = 0.1$, $M_2 = 0.3$, $h = 0.5$, $D_1 = C_1 = 1$, $\epsilon = \pi/6$. **Dashdot line crosses the real axis at** u_c **at an angle** $\pi/2 - \epsilon$. **Area between two solid lines is the analytical strip.**

The most important part for Weiner-Hopf problem is to factor the kernel into two split functions that are regular in certain half plane. In the case we have mentioned, such as Munt[3] and Gabard and Astley,[10] the factorization is implemented on a scalar that could be achieved in various ways.[11] But in our case, the process has to be done on a matrix in which the scalar splitting skills could not be easily exploited. In this paper, a commutative factorization of Weiner-Hopf kernel of Khrapkov type is utilized, the detail of which could be inferred in the appendix. Before the process of factoring, discussions are required for the properties of the kernel.

As we know, the dispersion relation and the characteristic equation could give the possible values of the wavenumbers. Under the consideration of the derivation above, it is evidently that these values are defined as solutions of $\det \mathbf{K}(u) = 0$, which means that the kernel $\mathbf{K}(u)$ contains the same information as the dispersion and characteristic equation. Therefore it is necessary to study the zeros of the kernel since each one of them represents an eigenmode of the problem.

A first group of zeros and poles are found when the dominator of the terms in $\mathbf{K}$ is zero, that is when $\mathrm{Y}'_m(\lambda_1\omega h)\mathrm{J}'_m(\lambda_1\omega) = \mathrm{J}'_m(\lambda_1\omega h)\mathrm{Y}'_m(\lambda_1\omega)$, which corresponds to the acoustic modes of the duct. Figure 2

shows the zeros and poles under certain circumstance. They are located close to the line crossed the real axis at $u_c = (u_1^+ + u_1^-)/2$ at an angle $\pi/2 - \epsilon$, away from the strip S.

Second group of zeros is related to the vortex sheet, in other words, the difference between the velocities in each layer. Therefore an expression of the zeros that is only influenced by velocity(with fixed radius) is expected, which makes the high frequency approximation more naturally. When $|\omega| \to \infty$, each component in $\mathbf{K}$ can be simplified using asymptotic forms of bessel functions for large arguments provided that $\lambda_1 \neq 0$ and $\lambda_2 \neq 0$.

$$\begin{aligned} det\mathbf{K} &= -D_1 D_2 (1-uM_1)^2 (1-uM_2)^2 \lambda_0^2 \lambda_1 \lambda_2 \cot[(1-h)\lambda_1\omega] \cot[\lambda_2\omega h - m\pi/2 - \pi/4] \\ &\quad + D_1 (1-uM_0)^2 (1-uM_1)^2 \lambda_0 \lambda_1 \lambda_2^2 \cot[(1-h)\lambda_1\omega] i \\ &\quad - D_2 (1-uM_0)^2 (1-uM_2)^2 \lambda_0 \lambda_1^2 \lambda_2 i \cot[\lambda_2\omega h - m\pi/2 - \pi/4] \\ &\quad + D_1^2 (1-uM_1)^4 \lambda_0^2 \lambda_2^2 \end{aligned} \tag{60}$$

If the imaginary part of λ_1 is positive or negative, $\cot[(1-h)\lambda_1\omega]$ can be approximated by i or $-i$ respectively. Similarly, if the imaginary part of λ_2 is positive or negative, $\cot[\lambda_2\omega h - m\pi/2 - \pi/4]$ can be approximated by i or $-i$ respectively. Then the zeros of $\det \mathbf{K} = 0$ are the solutions of:

$$(\lambda_1 + \lambda_0)(\lambda_1\lambda_0 + u^2) = 0, \text{or} \tag{61}$$

$$(\lambda_1 - \lambda_0)(\lambda_1\lambda_0 - u^2) = 0, \text{or} \tag{62}$$

$$(\lambda_2 + \lambda_1)(\lambda_1\lambda_2 + u^2) = 0, \text{or} \tag{63}$$

$$(\lambda_2 - \lambda_1)(\lambda_1\lambda_2 - u^2) = 0. \tag{64}$$

with different precedent conditions respectively. We would define $\nu = u^{-1}$ to simplify the solutions.

The solutions of $\lambda_1\lambda_0 + u^2 = 0$ are

$$\nu_{0,1} = \frac{M_0 + M_1}{2} \pm \frac{1}{2}\left[(M_1 - M_0)^2 + 4 - 4\sqrt{1 + (M_1 - M_0)^2}\right]^{\frac{1}{2}}. \tag{65}$$

The solutions of $\lambda_1\lambda_2 + u^2 = 0$ are

$$\nu_{6,7} = \frac{M_1 + M_2}{2} \pm \frac{1}{2}\left[(M_2 - M_1)^2 + 4 - 4\sqrt{1 + (M_2 - M_1)^2}\right]^{\frac{1}{2}}. \tag{66}$$

For subsonic flows the second term is always imaginary. The real part of the formula shows that the waves due to these zeros are moving at the average speed of the two streams. The imaginary part shows that the exponential growth of the waves is controlled by the differences of velocity between the two streams. If $M_0 \neq M_1$, only u_0 is a genuine zero of the kernel which represents the instability wave of the shear layer which is growing exponentially in the positive z direction. For the situation $M_1 \neq M_2$, u_6 has the same behavior.

The solutions of $\lambda_1\lambda_0 - u^2 = 0$ are:

$$\nu_{2,3} = \frac{M_0 + M_1}{2} \pm \frac{1}{2}\left[(M_1 - M_0)^2 + 4 + 4\sqrt{1 + (M_1 - M_0)^2}\right]^{\frac{1}{2}}. \tag{67}$$

The solutions of $\lambda_1\lambda_2 - u^2 = 0$ are:

$$\nu_{8,9} = \frac{M_1 + M_2}{2} \pm \frac{1}{2}\left[(M_2 - M_1)^2 + 4 + 4\sqrt{1 + (M_2 - M_1)^2}\right]^{\frac{1}{2}}. \tag{68}$$

These zeros are real, so is the corresponding λ_2, which does not satisfy the pre-conditions $\mathrm{Im}(\lambda_1) < 0$ or $\mathrm{Im}(\lambda_2) > 0$ that makes these zeros exist. We then conclude that they do not correspond to the zeros of the kernel.

The solutions of $\lambda_1 - \lambda_0 = 0$ are given by:

$$\nu_{4,5} = M_0 \pm M_1 C_1. \tag{69}$$

The solutions of $\lambda_2 - \lambda_1 = 0$ are given by:

$$\nu_{10,11} = M_1 \pm M_2 C_2. \tag{70}$$

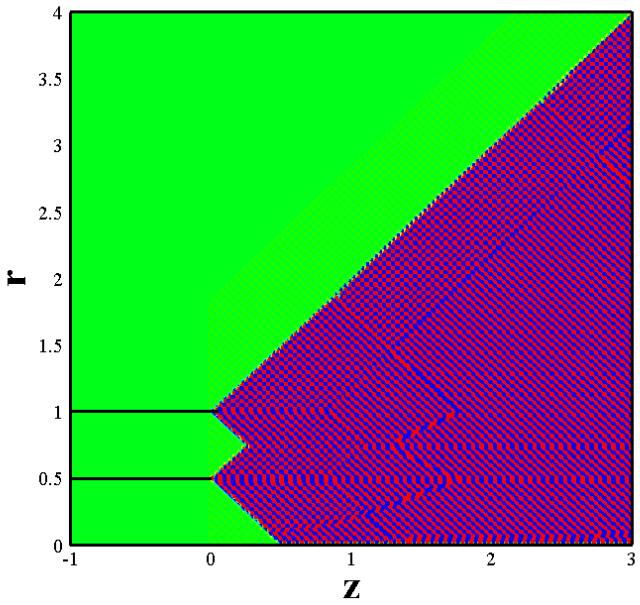

Figure 3. Near-field pressure contribution without eliminating instability wave. $\omega = 10$, $M_0 = 0.0$, $M_1 = 0.1$, $M_2 = 0.1$, $h = 0.5$.

These solutions are real thus with proper ω no instability would grow up. There is no solutions of $\lambda_1 + \lambda_0 = 0$ and $\lambda_2 + \lambda_1 = 0$.

In conclusion, there is two unstable zeros of the kernel due to the velocity mismatches of each shear layer. Figure 2 shows one of them, which usually lies in the strip that should be eliminated in the inverse transform integrations. Figure 3 show the theoretical solution of certain case without removing the unstable points. Instability waves grow directly from the beginning of each shear layer, within a wedge at 45° to the vortex sheet, which has already been demonstrated in the work by Morgan[7] and Crighton & Leppington.[8]

C. General solution

According to Khrapkov commutative factorization,[22,23] the detail of which would be given in appendix, we could get the split functions as following:

$$\mathbf{K} = \mathbf{K}^-\mathbf{K}^+(u-u_0)(u-u_6) = \mathbf{K}^+\mathbf{K}^-(u-u_0)(u-u_6). \tag{71}$$

Then equation (54) could be changed into the form

$$\frac{\omega(u-u_0)(u-u_6)}{\lambda_0^+(u)\lambda_1^+(u)\lambda_2^+(u)}\mathbf{K}^+(u)\mathbf{F}^+(u) = \lambda_0^-(u)\lambda_1^-(u)\lambda_2^-(u)\tilde{\mathbf{K}}^-(u)\mathbf{G}^+(u) + \lambda_0^-(u)\lambda_1^-(u)\lambda_2^-(u)\tilde{\mathbf{K}}^-(u)\mathbf{G}^-(u). \tag{72}$$

where $\tilde{\mathbf{K}}^{\pm}(u)$ represents the inverse matrix of $\mathbf{K}^{\pm}(u)$. $\tilde{\mathbf{K}}^{\pm}(u)$ and $\mathbf{K}^{\pm}(u)$ are all regular in $R_{\pm}$.

The left-hand side of equation (72) is regular in half plane below R^+, while the second term in the right-hand side is regular in half plane above R^-. For the first term, according to Eq. (48) and Eq. (49), a simple pole $u = \mu_{mn}^+$ exists in R^-. In order to eliminate the irregularity, we have to add an extra term on Eq. (72):

$$\frac{\omega(u-u_0)(u-u_6)\mathbf{K}^+(u)\mathbf{F}^+(u)}{\lambda_0^+(u)\lambda_1^+(u)\lambda_2^+(u)} - \lambda_0^-(\mu_{mn}^+)\lambda_1^-(\mu_{mn}^+)\lambda_2^-(\mu_{mn}^+)\tilde{\mathbf{K}}_-(\mu_{mn}^+)\mathbf{G}^+(u) \tag{73}$$

$$= [\lambda_0^-(u)\lambda_1^-(u)\lambda_2^-(u)\tilde{\mathbf{K}}_-(u) - \lambda_0^-(\mu_{mn}^+)\lambda_1^-(\mu_{mn}^+)\lambda_2^-(\mu_{mn}^+)\tilde{\mathbf{K}}_-(\mu_{mn}^+)]\mathbf{G}^+(u) \tag{74}$$

$$+\lambda_0^-(u)\lambda_1^-(u)\lambda_2^-(u)\tilde{\mathbf{K}}_-(u)\mathbf{G}^-(u). \tag{75}$$

This equation above would be only satisfied in the strip S.

Here is another key step in Weiner-Hopf technique: by analytical continuation, both sides of the above equation equal to an regular function, say $E(u)$ on the whole complex plane. As $|u| \to \infty$, $G_1^+(u)$ and $G_2^+(u)$ behave with the order $O(u^{-1})$ and $\lambda_i^{\pm}(u)$ with the order $O(u^{1/2})$. Considering Eq. (56)-(59), $K_{ij} = O(u^4)$, and it could be easily shown that under Khrapkov commutative factorization $\mathbf{K}_{\pm}(u) = O(u^{\pm 1})$. At the trailing edge Kutta condition is applied that $\psi(1, z) = O(z^{3/2})$ as $|z| \to 0^+$, which results in $F_{1,2}^+(u) = O(u^{-5/2})$ as $|u| \to \infty$. Therefore, $E(u) = O(u^{-1})$ as $|u| \to \infty$ which means that by analytical continuation $E(u)$ is zero and the whole plane. We can get

$$\mathbf{F}^+(u) = \frac{\lambda_0^+(u)\lambda_1^+(u)\lambda_2^+(u)\lambda_0^-(\mu_{mn}^+)\lambda_1^-(\mu_{mn}^+)\lambda_2^-(\mu_{mn}^+)\tilde{\mathbf{K}}_+(u)\tilde{\mathbf{K}}_-(\mu_{mn}^+)\mathbf{G}^+(u)}{\omega(u-u_0)(u-u_6)}. \tag{76}$$

Then we could figure out both $F_1^+(u)$ and $F_2^+(u)$ thus $A(u)$, $B(u)$, $C(u)$ and $D(u)$ are determined, so is the solution.

By taking advantage of inverse Fourier transform, $\beta(r, u)$ could be obtained, which would lead to the solution of the diffracted field:

$$\psi(r, z) = \frac{\omega}{2\pi} \int_\Gamma \beta(r, u) \exp(i\omega u z) du. \tag{77}$$

where the path of integration Γ is aline from $-\infty e^{-i\epsilon}$ to $+\infty e^{+i\epsilon}$ in the strip.

For the problem at hand, we would take the limit $\epsilon \to 0$ and the path of integration is then deformed. As we can see in figure 2, when $\epsilon \to 0$, Γ turns close to the real axis that it would encounter the unstable points, which violates the analytic continuity. Therefore the path of integration needs to be deformed around the unstable points. According to Reinstra,[24] causality condition is guaranteed since it is consistent with the solution including the instability wave. The path of integration for real frequency ω goes from $-\infty + 0i$ to $+\infty - 0i$, crosses the real axis at u_c and is intended to include the instability wave.

In scalar kernel cases, the statement above is obvious and has been verified in lots of works. While in matrix kernel case, since two shear layers exist, the conclusion that asymptote across u_c needs extra explanation. Figure 4 is a schematic diagram. Figure 4(a) is for scalar kernel case while (b) for our matrix case. For scalar case there is only one shear layer. Thus the inverse integral path could behave as pictured that right-going modes and unstable points are included. For our case two shears layer exist. If each layer is considered separately, they would have different integral paths for different sets of zeros and poles. Figure 4(b) shows two integration path $\Gamma_{1,2}$. Hollow circle are sets of zeros and poles for Γ_1 and solid circle are sets of zeros and poles for Γ_2. In certain situations, like figure 4(b), the right-going modes for one layer and the left-going modes for the other one could have intersection region, which makes it difficult for choosing integral path when the two layers are coupled. In order to avoid such problem we make the regular strip S as small as possible that no "bad points" exist.

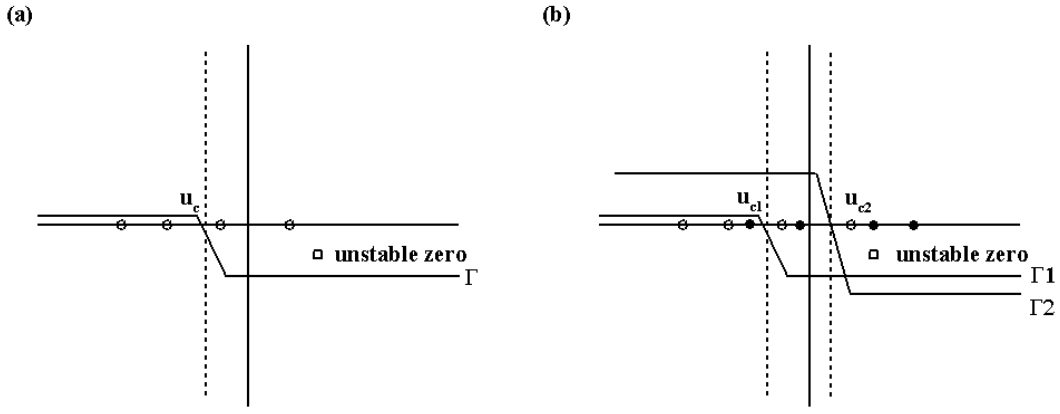

Figure 4. Integral path of the inverse Fourier transform. (a) is for scalar kernel case, (b) is for matrix kernel case. Hollow circle are sets of zeros and poles for one shear layer and solid circle are sets of zeros and poles for another shear layer. Only points on the real axis are drawn.

$$\psi(r,z) = \frac{\omega}{2i\pi}\int_\Gamma \frac{(1-uM_0)F_1(u)}{\lambda_0}T_0(r,u)\exp(i\omega uz)du, \quad r>1, \tag{78}$$

$$\psi(r,z) = \frac{\omega}{2i\pi}\int_\Gamma \frac{(1-uM_1)}{\lambda_1}[F_1(u)T_{11}(r,u)+F_2(u)T_{12}(r,u)]\exp(i\omega uz)du, \quad h<r<1, \tag{79}$$

$$\psi(r,z) = \frac{\omega}{2i\pi}\int_\Gamma \frac{(1-uM_2)F_2(u)}{\lambda_2}T_2(r,u)\exp(i\omega uz)du, \quad r<h. \tag{80}$$

$$p(r,z) = \frac{\omega^2}{2\pi}\int_\Gamma \frac{(1-uM_0)^2F_1(u)}{\lambda_0}T_0(r,u)\exp(i\omega uz)du, \quad r>1, \tag{81}$$

$$p(r,z) = \frac{\omega^2}{2\pi}\int_\Gamma \frac{(1-uM_1)^2}{\lambda_1}[F_1(u)T_{11}(r,u)+F_2(u)T_{12}(r,u)]\exp(i\omega uz)du, \quad h<r<1, \tag{82}$$

$$p(r,z) = \frac{\omega^2}{2\pi}\int_\Gamma \frac{(1-uM_2)^2F_2(u)}{\lambda_2}T_2(r,u)\exp(i\omega uz)du, \quad r<h. \tag{83}$$

where

$$T_0(r,u) = \frac{H_m^{(1)}(\lambda_0\omega r)}{H_m^{(1)\prime}(\lambda_0\omega)}, \tag{84}$$

$$T_{11}(r,u) = \frac{J_m(\lambda_1\omega r)Y_m'(\lambda_1\omega h)-J_m'(\lambda_1\omega h)Y_m(\lambda_1\omega r)}{J_m'(\lambda_1\omega)Y_m'(\lambda_1\omega h)-J_m'(\lambda_1\omega h)Y_m'(\lambda_1\omega)}, \tag{85}$$

$$T_{12}(r,u) = \frac{Y_m(\lambda_1\omega r)J_m'(\lambda_1\omega)-J_m(\lambda_1\omega r)Y_m'(\lambda_1\omega)}{J_m'(\lambda_1\omega)Y_m'(\lambda_1\omega h)-J_m'(\lambda_1\omega h)Y_m'(\lambda_1\omega)}, \tag{86}$$

$$T_2(r,u) = \frac{J_m(\lambda_2\omega r)}{J_m'(\lambda_2\omega h)}. \tag{87}$$

D. Far-field

For the far-field , $\psi(r,z)$ and $p(r,z)$ at $r>1$ have been taken into consideration, which can both be written in the from:

$$q(r,z) = \frac{\omega}{2\pi}\int Q(u)H_m^{(1)}(\lambda_0\omega r)\exp(i\omega uz)du, \tag{88}$$

where

$$Q(u) = \begin{cases} \frac{(1-uM_0)F_1(u)}{i\lambda_0(u)H_m^{(1)\prime}(\lambda_0\omega)} & if \quad q=\psi, \\ \frac{\omega(1-uM_0)^2F_1(u)}{\lambda_0(u)H_m^{(1)\prime}(\lambda_0\omega)} & if \quad q=p. \end{cases} \tag{89}$$

Introducing a new coordinates defined as: $r=\hat{R}\sin\hat{\theta}$, $z=\sqrt{1-M_0^2}\hat{R}\cos\hat{\theta}$, $\omega=\sqrt{1-M_0^2}\hat{\omega}$, $u=(\tau-M_0)/(1-M_0^2)$, which is Lorentz transform. Thus in the new system q can be written as :

$$\begin{aligned} q(\hat{R},\hat{\theta}) &= \frac{\sqrt{1-M_0^2}\hat{\omega}}{2\pi}\int Q\left(\frac{\tau-M_0}{1-M_0^2}\right)H_m^{(1)}(\lambda_0\sqrt{1-M_0^2}\hat{\omega}\hat{R}\sin\hat{\theta}) \\ &\quad \cdot\exp\left(i\sqrt{1-M_0^2}\hat{\omega}\frac{\tau-M_0}{1-M_0^2}\sqrt{1-M_0^2}\hat{R}\cos\hat{\theta}\right)d\frac{\tau-M_0}{1-M_0^2} \\ &= \frac{\hat{\omega}\exp\left(-i\hat{\omega}\hat{R}M_0\cos\hat{\theta}\right)}{2\pi\sqrt{1-M_0^2}}\int Q(u)H_m^{(1)}\left(\hat{\omega}\hat{R}\sqrt{1-M_0^2}sin\hat{\theta}\right)\exp\left(i\hat{\omega}\hat{R}\tau\cos\hat{\theta}\right)d\tau. \end{aligned} \tag{90}$$

The relation $\lambda_0\sqrt{1-M_0^2}=\sqrt{1-\tau^2}$ is used during derivation. Expanding $H_m^{(1)}(x)$ we have:

$$H_m^{(1)}(x) = \sqrt{\frac{2}{\pi x}}\exp\left(i(x-\frac{2}{\pi}m-\frac{\pi}{4})\right), \tag{91}$$

then equation Eq. (90) turns into:

$$q(\hat{R},\hat{\theta}) = \frac{\hat{\omega}\exp\left(-i\hat{\omega}\hat{R}M_0\cos\hat{\theta} - \frac{2}{\pi}mi - \frac{\pi}{4}i\right)}{2\pi\sqrt{1-M_0^2}}\sqrt{\frac{2}{\pi\hat{\omega}\hat{R}}sin\hat{\theta}} \cdot \int \frac{Q(u)}{(1-\tau^2)^{1/4}}\exp\left[i\hat{\omega}\hat{R}(\sqrt{1-\tau^2})sin\hat{\theta} + \tau\cos\hat{\theta}\right]. \quad (92)$$

Taking advantage of Method of Stationary Phase, we could estimate q:

$$q = \frac{Q(u_s)}{\pi\hat{R}\sqrt{1-M_0^2}}\exp\left[i\hat{\omega}\hat{R}(1-M_0\cos^2\hat{\theta}) - i(m+1)\frac{\pi}{2}\right]. \quad (93)$$

Introducing spherical coordinate $r = Rsin\theta$,$z = R\cos\theta$, which leads to $\cos\hat{\theta} = \cos\theta\sqrt{1-M_0^2sin^2\theta}$, $\hat{R} = R/\sqrt{\frac{1-M_0^2}{1-M_0^2sin^2\theta}}$. Substituting into equation Eq. (92) we have

$$q(R,\theta) = \frac{Q(u_s)}{\pi R\sqrt{1-M_0^2sin^2\theta}}\exp[i\omega RS(\theta) - i(m+1)\frac{\pi}{2}]. \quad (94)$$

where $S(\theta) = (\sqrt{1-M_0^2sin^2\theta} - M_0\cos\theta)/1-M_0^2$, $u_s = (\cos\hat{\theta} - M_0)/(1-M_0^2)$.

The directivity functions D_p and D_ψ for pressure and velocity is then defined as $D_p(\theta) = |p|R$ and $D_\psi(\theta) = |\psi|R$.

IV. Results

In order to confirm the performance of the theoretical solution, a numerical simulation is carried out as well. LEE equations are solved in cylindrical coordinates for sound wave propagation.[14] In Fig 5, the settings are depicted. Non-dimensional geometries and coefficient are the same for numerical case and theoretical case. Sixth order pre-factored compact scheme is employed to calculate spatial derivatives. Fourth-order 4/6-stage explicit Runge-Kutta scheme[25] was used for time integration. Slip-wall boundary condition was utilized for the hard duct walls. A buffer zone was applied to absorb the reflective spurious waves, as well as to accommodate incoming modal waves. With no loss of generality, the ambient flow speed is set to zero for simplicity. The data on the FW-H integral surface are recorded and then used to solve FW-H equation, which gives the far-field solution.

Figure 6(a) gives the cross-section pressure contour of the theoretical solution and 6(b) gives that of the the numerical solution for comparison. Inside the bypass duct the incident wave remains while after the duct end the diffraction effect of the trailing edge, or say velocity mismatch, is clear. The two results show the quite the same pressure distribution, indicating that the theoretical model we have provided is accurate.

Figure 7 is a comparison of farfield directivity patterns for different cases. Our solution is illustrated in black line and the numerical result is illustrated in red line. Theoretical solutions using scalar Weiner-Hopf kernel are also pictured in figure 7. Blue line represents the result of Gabard and Astley's case and green line represents the result of Munt's case under same flow coefficients, the geometry of which is provided in figure 1. In general our result agrees with the numerical solution at the low angle region. The oscillation at high angle region of numerical solution is due to the buffer zone we have used, which should not been taken into consideration in comparison. Our solution shows an energy drop at the angle around 80° while numerical solution is rather smooth. We think it may be influenced by the spatial difference method we used. Munt's results and Gabard and Astley's results are overall similar to our solution besides the energy drop angle and degree. The geometry differences are supposed to be the main reason. In Gabard and Astley's case there is no inner pipe but an inner hub, which makes the effect of inner shear layer disappear. Taking two velocity mismatches into account is our main contribution in this work.

V. Summary

Spinning sound radiation from a semi-infinite annular duct is investigated in this work, representing a further step from previous efforts. It serves as an idealized model for the sound radiated from the bypass

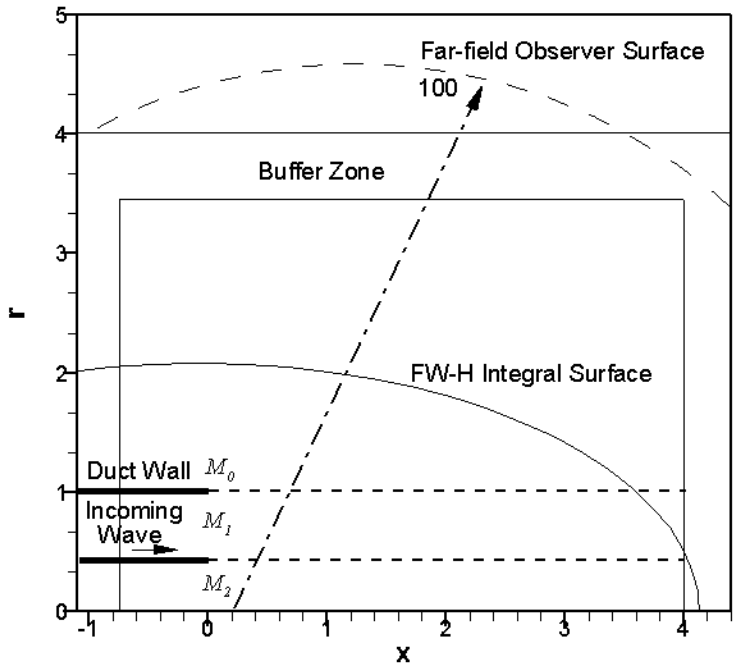

Figure 5. Schematic of nondimensionalized problem setup for semi-infinite duct geometry and subsonic jet flow. Far-field distance is not scaled.

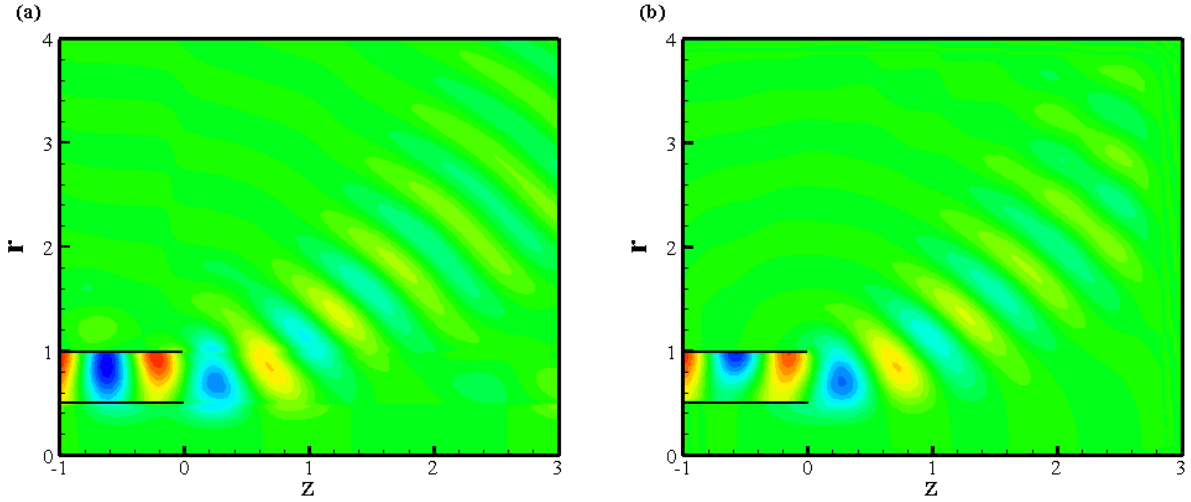

Figure 6. Nearfield pressure distribution for mode $(4, 1)$, $\omega = 10$, $M_0 = 0$, $M_1 = 0.1$, $M_2 = 0.3$. **(a) WH solution, (b) LEE solution.**

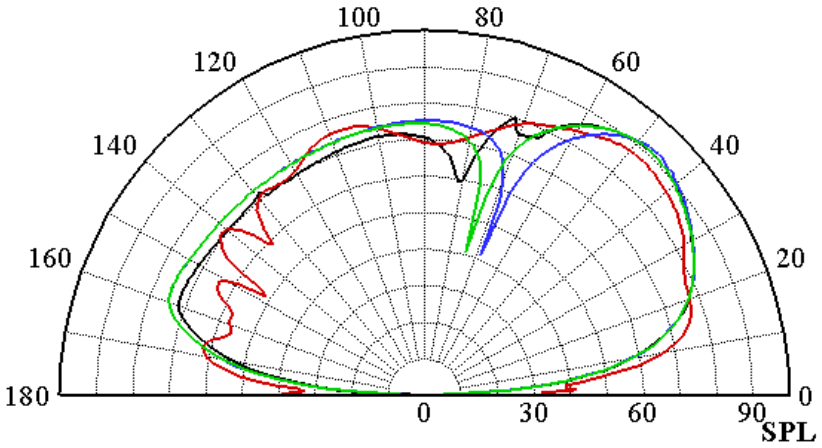

Figure 7. Farfield directivity pattern for mode $(4,1)$, $\omega = 10$, $M_0 = 0$, $M_1 = 0.1$, $M_2 = 0.3$. **Black line for WH solution, red line for LEE solution, blue line for Gabard and Astley's case with no** M_2**, green line for Munt's with no** M_2**.**

duct of a turbofan engine. Unlike the annular duct with inner hub, our case has an inner pipe with outlet flow in presence, which makes two shear layers after the open end instead of one.

Weiner-Hopf method has been used as the main mathematical tool. In our work, due to the two shear layers, Weiner-Hopf kernel is a matrix, which makes the discussion quite different and complex from other relative work where the kernel is scalar. The instability wave introduced by the vortex shedding from the two trailing edge is studied, with full Kutta condition applied. It has been pointed out that two coupled velocity mismatches may cause the confliction of inverse transform integration path, which needs extra treatment to exclude the unstable point.

Numerical verification solving linearized Euler equation has been carried out. Both far- and near-field solutions are compared. The results indicates that our model agrees well with the numerical solution. Comparison between different geometries is also conducted, concluding that the influence of geometry is significance.

Our model settle the problem of sound radiating through two coupled shear layers, which is a better representative of the bypass engine issue. In this way, general characters of sound radiation from realistic turbofan exhausts could be simulated quickly and robustly.

Acknowledgments

This work is supported by National Science Foundation of China (Grants 11172007 and 11322222) and AVIC Commercial Aircraft Engine Co., Ltd.

Appendix

According to Abrahams,[22] by defining

$$a_0 = \frac{K_{11} + K_{22}}{2(u-u_0)(u-u_6)}, a_1 = \frac{K_{11} - K_{22}}{2(u-u_0)(u-u_6)}. \tag{95}$$

$$l = 1, m = \frac{2K_{12}}{K_{11} - K_{22}}, n = \frac{2K_{21}}{K_{11} - K_{22}}. \tag{96}$$

Then $\mathbf{K}$ could be written in the form

$$\mathbf{K} = a_0\mathbf{I} + a_1\mathbf{E}. \tag{97}$$

where $\mathbf{I}$ is the unit matrix and

$$\mathbf{E} = \begin{bmatrix} l & m \\ n & -l \end{bmatrix}. \tag{98}$$

$\mathbf{E}$ has the property that $\mathbf{E}^2 = q^2\mathbf{I}$, where

$$q^2 = l^2 + mn. \tag{99}$$

q^2 is an entire function, $\mathrm{tr}\mathbf{E} = 0$ and $\det\mathbf{K} = a_0^2 - a_1^2 q^2 \neq 0$. σ is introduced by

$$\sigma = \frac{1}{2q}\ln(\frac{\gamma_1}{\gamma_2}) \tag{100}$$

where γ_i is the eigenvalue of $\mathbf{K}$:

$$\gamma_1 = a_0 + a_1 q, \tag{101}$$

$$\gamma_2 = a_0 - a_1 q. \tag{102}$$

We could define

$$\ln\gamma_{1\pm} = \frac{1}{2\pi i}\int_{C_\pm} \frac{\ln\gamma_1(\xi)}{\xi - u} d\xi, \tag{103}$$

$$\ln\gamma_{2\pm} = \frac{1}{2\pi i}\int_{C_\pm} \frac{\ln\gamma_2(\xi)}{\xi - u} d\xi, \tag{104}$$

$$\sigma_\pm = \frac{1}{2\pi i}\int_{C_\pm} \frac{\sigma(\xi)}{\xi - u} d\xi. \tag{105}$$

where the path of integration $C_\pm$ go from $-\infty\exp(-i\epsilon)$ to $+\infty\exp(-i\epsilon)$ in the strip S, with C_+ and C_- above and below u respectively.

Then the factorization is achieved

$$\mathbf{K}_\pm = \sqrt{\gamma_{1\pm}\gamma_{2\pm}}\left[\mathbf{I}\cosh(q\sigma_\pm) + \frac{\mathbf{E}}{q}\sinh(q\sigma_\pm)\right] \tag{106}$$

Kernel $\mathbf{K}$ has been factored into two parts $\mathbf{K} = \mathbf{K}^-\mathbf{K}^+(u-u_0)(u-u_6) = \mathbf{K}^+\mathbf{K}^-(u-u_0)(u-u_6)$ with both $\det\mathbf{K}^+$ and $\det\mathbf{K}^-$ are not equal to zero. Thus both of them are reversible:

$$(\mathbf{K}^+)^{-1} = \frac{1}{\sqrt{\gamma_{1+}\gamma_{1+}}}\left[\mathbf{I}\cosh(q\sigma_+) - \frac{\mathbf{E}}{q}\sinh(q\sigma_+)\right] \doteq \tilde{\mathbf{K}}_+ \tag{107}$$

$$(\mathbf{K}^-)^{-1} = \frac{1}{\sqrt{\gamma_{1-}\gamma_{1-}}}\left[\mathbf{I}\cosh(q\sigma_-) - \frac{\mathbf{E}}{q}\sinh(q\sigma_-)\right] \doteq \tilde{\mathbf{K}}_- \tag{108}$$

$\tilde{\mathbf{K}}_\pm$ are regular in half plane $R^\pm$.

References

[1]Levine, H. and Schwinger, J., "On the Radiation of Sound from an Unflanged circular pipe," *Physics Review*, Vol. 30, 1948, pp. 383–406.

[2]Carrier, G., "Sound transmission from a tube with flow," *Quarterly of Applied Mathematicas*, Vol. 13, 1956, pp. 457–461.

[3]Munt, R., "Acoustic Radiation from a Circular Cylinder in a Subsonic Stream," *Journal of the Institute of Mathematics and its Application*, Vol. 16, No. 1, 1975, pp. 1–10.

[4]Reinstra, S., "Acoustic Radiation from a Semi-infinite Annular Duct in a Uniform Subsonic Mean Flow," *Journal of Sound and Vibration*, Vol. 94, No. 2, 1984, pp. 267–288.

[5]Cargill, A., "Low frequenct acoustic radiation from a jet pipe," *Journal of Sound and Vibration*, Vol. 83, 1982, pp. 339–354.

[6]Cargill, A., "The radiation of high frequency sound out of a jet pipe," *Journal of Sound and Vibration*, Vol. 83, 1982, pp. 313–337.

[7]Morgan, J., "the interaction of sound with a semi-infinite vortex sheet," *Quarterly Journal of Mechanics and Applied Mechanics*, Vol. 27, 1974, pp. 465–487.

[8]Crighton, D., "Radiation properties of semi-infinite vortex sheet: the initial value problem," *Journal of Fluid Mechanics*, Vol. 64, No. 2, 1974, pp. 393–414.

[9]Bechert, D. and Pfizenmainer, "Optical compensation measurements on the unsteady exit condition at a nozzel discharge edge," *Journal of Fluid Mechanics*, Vol. 71, 1971, pp. 123–144.

[10]Gabard, G. and Astley, R., "Theoretical Model for Sound Radiation from Annular Jet Pipes: Far-and Near-field Solutions," *Journal of Fluid Mechanics*, Vol. 549, No. 315-41, 2006, pp. 1103–1124.

[11]Noble, B., *Methods Based on the Weiner-Hopf Technique*, Pergamon Press, London, 1958.

[12]Taylor, M., Crighton, D., and Cargill, A., "The low frequency aeroacoustics of buried nozzle systems," *Journal of sound and vibration*, Vol. 163, No. 3, 1993, pp. 493–526.

[13]Veitch, B. and Peake, N., "Acoustic propagation and scattering in the exhaust flow from coaxial cylinders," *Journal of Fluid Mechanics*, Vol. 613, 2008, pp. 275–307.

[14]Huang, X., Chen, X. X., Ma, Z. K., and Zhang, X., "Efficient Computation of Spinning Modal Radiation Through an Engine Bypass Duct," *AIAA Journal*, Vol. 46, No. 6, 2008, 1413–1423.

[15]Kok and Johan, C., "Computation of sound radiation from cylindrical ducts with jets using a high-order finite-volume method," *AIAA Paper*, Vol. 3489, 2007, pp. 2007.

[16]Iob, A., Arina, R., and Schipani, C., "Frequency-domain linearized Euler model for turbomachinery noise radiation through engine exhaust," *AIAA journal*, Vol. 48, No. 4, 2010, pp. 848–858.

[17]Reboul, G. and Polacsek, C., "Towards Numerical Simulation of Fan Broadband Noise Aft Radiation from Aeroengines," *AIAA journal*, Vol. 48, No. 9, 2010, pp. 2038–2048.

[18]Jones, D. and Morgan, J., "The Instability due to Acoustic Radiation striking a Vortex Sheet on a Supersonic Stream," *Proceedings of the Royal Society of Edinburgh. Section A. Mathematical and Physical Sciences*, Vol. 71, No. 02, 1973, pp. 121–140.

[19]Jones, D., "The scattering of sound by a vortex sheet," *IMA Journal of Applied Mathematics*, Vol. 15, No. 1, 1975, pp. 33–57.

[20]Morgan, J., "The interaction of sound with a semi-infinite vortex sheet," *The Quarterly Journal of Mechanics and Applied Mathematics*, Vol. 27, No. 4, 1974, pp. 465–487.

[21]Morgan, J., "The interaction of sound with a subsonic cylindrical vortex layer," *Proceedings of the Royal Society of London. A. Mathematical and Physical Sciences*, Vol. 344, No. 1638, 1975, pp. 341–362.

[22]Abrahams, I., "On the Non-Commutative Factorization of Wiener-Hopf Kernels of Khrapkov Type," *Proceedings of the Royal Society of London. Series A: Mathematical, Physical and Engineering Sciences*, Vol. 454, No. 1974, 1998, pp. 1719–1743.

[23]Manzhirov, A. and Polianin, A., *Handbook of Mathematics for Engineers and Scientists*, Chapman and Hall/CRC, 2007.

[24]Reinstra, S. and Hirschberg, A., "An introduction to acoustics," *Report IWDE*, 2001, pp. 92–06.

[25]F.Q. Hu, M. H. and Manthey, J., "Low-dissipation and low-dispersion Runge-Kutta schemes for computational acoustics," *Journal of Computational Physics*, Vol. 124, No. 1, 1996, pp. 177–191.